Phase Noise Effect on MIMO-OFDM Systems with Common and Independent Oscillators

Chen, Xiaoming; Wang, Hua; Fan, Wei; Zou, Yaning ; Wolfgang, Andreas ; Svensson, Tommy; Luo, Jian

Published in:
Wireless Communications and Mobile Computing (Print)

DOI (link to publication from Publisher):
10.1155/2017/8238234

Publication date:
2018

Document Version
Publisher's PDF, also known as Version of record

Hindawi
Wireless Communications and Mobile Computing
Volume 2017, Article ID 8238234, 12 pages
https://doi.org/10.1155/2017/8238234

WILEY | Hindawi

Research Article

Phase Noise Effect on MIMO-OFDM Systems with Common and Independent Oscillators

Xiaoming Chen,[1] Hua Wang,[2] Wei Fan,[3] Yaning Zou,[4] Andreas Wolfgang,[5] Tommy Svensson,[6] and Jian Luo[7]

[1]*School of Electronic and Information Engineering, Xi'an Jiaotong University, Xi'an 710049, China*
[2]*Keysight Laboratories, Keysight Technologies, Inc., 9220 Aalborg, Denmark*
[3]*Department of Electronic Systems, Aalborg University, 9000 Aalborg, Denmark*
[4]*Vodafone Chair Mobile Communications Systems, Dresden University of Technology, 01062 Dresden, Germany*
[5]*Qamcom Research & Technology AB, 41285 Gothenburg, Sweden*
[6]*Department of Electrical Engineering, Chalmers University of Technology, 41296 Gothenburg, Sweden*
[7]*Huawei Technologies Duesseldorf GmbH, 80992 Munich, Germany*

Correspondence should be addressed to Wei Fan; wfa@es.aau.dk

Received 26 July 2017; Revised 13 October 2017; Accepted 22 October 2017; Published 12 November 2017

Academic Editor: Jose F. Monserrat

The effects of oscillator phase noises (PNs) on multiple-input multiple-output (MIMO) orthogonal frequency division multiplexing (OFDM) systems are studied. It is shown that PNs of common oscillators at the transmitter and at the receiver have the same influence on the performance of (single-stream) beamforming MIMO-OFDM systems, yet different influences on spatial multiplexing MIMO-OFDM systems with singular value decomposition (SVD) based precoding/decoding. When each antenna is equipped with an independent oscillator, the PNs at the transmitter and at the receiver have different influences on beamforming MIMO-OFDM systems as well as spatial multiplexing MIMO-OFDM systems. Specifically, the PN effect on the transmitter (receiver) can be alleviated by having more transmit (receive) antennas for the case of independent oscillators. It is found that the independent oscillator case outperforms the common oscillator case in terms of error vector magnitude (EVM).

1. Introduction

Due to the spectrum congestion in the lower microwave frequency range, millimeter wave (mmWave) communications have received a lot of attention due to the broad bandwidth. Multiple-input multiple-output (MIMO) techniques are usually employed for the radio access application, to overcome the high propagation attenuation in mmWave bands [1–3] and to enable high throughput [4, 5]. The orthogonal frequency division multiplexing (OFDM) technique [6] (that has been adopted in many modern communication systems) is recently chosen to be the main waveform for 5G communications below 40 GHz [7].

It is well-known that OFDM systems are sensitive to oscillator phase noises (PNs) that increase with increasing (carrier) frequency [8, 9]. The PN effects on OFDM or MIMO-OFDM systems have been extensively studied in the literature [10–26]. Most of the works assume free-running oscillators, except for [10–13], where phase locked loop (PLL) based oscillators were also assumed. Most of the studies assume a common oscillator for all the transmit (receive) antennas, except for [12, 24–26], where independent oscillators (i.e., each antenna is equipped with a different oscillator) were also considered. (The independent oscillator case is also considered for single carrier systems in [27, 28].) Moreover, most works did not distinguish different effects of PNs on the transmitter (Tx PN) and on the receiver (Rx PN), except for [16] where the effects of PNs of free-running (common) oscillators on receivers and transmitters were analyzed separately. The variance of the PN of a free-running oscillator increases with time. As the PN grows large, common phase error (CPE) correction (that is necessary for reliable data detection) tends to reduce the signal-to-noise ratio (SNR) [23]. Therefore, in practice the PLL is usually used to stabilize the PN. As a result,

we assume PLL-based oscillators in this work for simulations and verifications (even though the analysis is applicable to both free-running and PLL-based oscillators). In mmWave MIMO systems, distribution of the high frequency clock signal of a common oscillator for all the transmit/receive antennas may cause high attenuation and waveform distortion, especially for large antenna arrays. To avoid this problem, an independent oscillator can be used for each antenna (at the cost of increased complexity). Nevertheless, the common oscillator is still the most popular assumption in the literature. In this work, we consider both common oscillators and independent oscillators at the transmitter and the receiver and compare their impairments on MIMO-OFDM systems.

We evaluate the PN effect on the mmWave MIMO-OFDM system in terms of the error vector magnitude (EVM) [21, 27, 29], which is a popular performance metric for hardware impairment evaluations, especially in the industry. A conference version of this paper has been published in [30], where the study was confined to single-stream beamforming OFDM systems. In this paper, we extend the work by including the spatial multiplexing OFDM systems as well. Spatial multiplexing means transmitting multiple spatial streams simultaneously in the same band. Note that, in the literature, sometimes it is also referred to as adaptive beamforming with multiple layers (streams), for example, [31]. In this work, beamforming refers to single-stream beamforming in order to distinguish it from spatial multiplexing. It is noted that the (digital/analog) hybrid beamforming [5] is the most popular assumption for mmWave cellular communications. Nevertheless, other beamforming/precoding architectures are also considered in practice. For example, fully digital schemes with small MIMO orders and high gain antennas are used for mmWave backhauling in the industry.

New Contributions and Relation to Previous Work. It is shown in this work that, *for the common oscillator case*, Tx PN and Rx PN have the same level of influence on the beamforming OFDM system (in terms of EVM), yet different levels of influences on the singular value decomposition (SVD) based spatial multiplexing OFDM system (in the latter case, the conclusions are the same as in [16], where open-loop spatial multiplexing MIMO-OFDM systems with zero-forcing (ZF) decoders are considered). These findings (including the link between SVD-based spatial multiplexing OFDM and open-loop spatial multiplexing MIMO-OFDM system with ZF decoder) have not been shown in the previous literature. It is also shown that, *for the independent oscillator case*, Tx PN and Rx PN have different levels of influences on the beamforming and spatial multiplexing OFDM systems, whose adverse effect reduces as the number of antennas increases. Interestingly, it was reported in [28] that the effect of Rx PNs of independent oscillators reduces with increasing receive antennas for single carrier MIMO systems with maximum ratio combining. In this work, we show that the effect of PNs of independent oscillators can be alleviated with more antennas at either Tx or Rx side for both beamforming and SVD-based spatial multiplexing MIMO-OFDM systems. Moreover, our results show that the independent oscillator case can achieve better EVM performance than the common oscillator case. Finally, it is noted that, although digital beamforming is assumed for tractable analysis, the findings hold for hybrid beamforming [5] as well. This is rather intuitive if one regards each antenna in our analysis as a (analog) phase-controlled subarray in hybrid beamforming. This is verified by hybrid beamforming simulations using a sophisticated mmWave channel model.

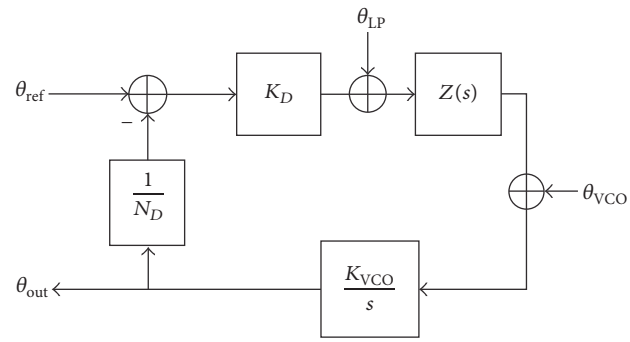

Figure 1: Phase noise model of PLL-based oscillator.

The rest of the paper is organized as follows. Section 2 presents the system models. PN effects of common and independent oscillators on beamforming and spatial multiplexing OFDM systems are derived and discussed separately in Section 3. Section 4 verifies the analytical results of the previous section by simulations. Finally, Section 5 concludes this paper.

Notations. Throughout this paper, $*$, T, and H denote complex conjugate, transpose, and Hermitian operators, respectively. Lower case bold letter ($\mathbf{x}$) and upper case bold letter ($\mathbf{X}$) represent column vector and matrix, respectively. $\mathbf{I}_M$ is the $M \times M$ identity matrix. diag($\mathbf{x}$) denotes the diagonal matrix whose diagonal elements are given by $\mathbf{x}$. tr($\mathbf{X}$) denotes the trace of $\mathbf{X}$. $\otimes$ denotes the Kronecker product.

2. System Model

2.1. Phase Noise Model. In this work, we consider the PLL-based oscillator that is used ubiquitously in practical transceivers. The PN of the PLL-based oscillator consists of three main noise sources, that is, noises from the reference oscillator θ_{ref}, the phase-frequency detector, the loop filter θ_{LP}, and the voltage controlled oscillator (VCO) θ_{VCO}, as shown in Figure 1. The Laplace transform of the PN of the PLL-based oscillator is given as [9]

$$\theta_{\text{out}}(s) = \frac{N_D K_{\text{VCO}} Z(s) \left(K_D \theta_{\text{ref}}(s) + \theta_{\text{LP}}(s)\right)}{sN_D + K_D K_{\text{VCO}} Z(s)} + \frac{sN_D \theta_{\text{VCO}}(s)}{sN_D + K_D K_{\text{VCO}} Z(s)}, \tag{1}$$

where K_D denotes the gain of the phase-frequency detector, K_{VCO} represents the sensitivity of the VCO, $Z(s)$ represents

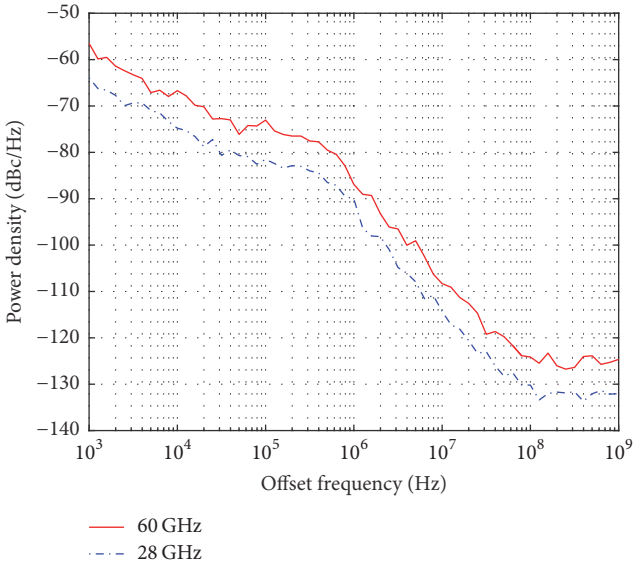

FIGURE 2: PSD of the carrier phase noise.

the loop filter, and $1/N_D$ is the frequency divider [9]. The noise sources include both white noise (thermal noise) and colored noise (flicker noise) [8]. The detailed modeling parameters are listed in Table 4-2 of [9]. As an example, Figure 2 shows the estimated power spectral density (PSD) of the carrier phase noise [11] (using the periodogram method with 2×10^8 PN samples) at 28 and 60 GHz, respectively.

2.2. MIMO-OFDM System. The MIMO-OFDM system with N_R receive antennas, N_T transmit antennas, and N OFDM subcarriers can be expressed as

$$\mathbf{y} = \mathbf{H}\mathbf{x} + \mathbf{w}, \tag{2}$$

where $\mathbf{H}$ is an $N_R N \times N_T N$ block diagonal channel matrix whose kth diagonal block entry $\mathbf{H}_k$ is the $N_R \times N_T$ MIMO channel matrix of the channel transfer functions at the kth subcarrier, $\mathbf{x} = \left[\mathbf{x}_1^T \ \mathbf{x}_2^T \ \cdots \ \mathbf{x}_N^T\right]^T$ is the $N_T N \times 1$ frequency-domain signal vector with $\mathbf{x}_k$ denoting the $N_T \times 1$ transmitted signal vector at the kth subcarrier, $\mathbf{y} = \left[\mathbf{y}_1^T \ \mathbf{y}_2^T \ \cdots \ \mathbf{y}_N^T\right]^T$ is the $N_R N \times 1$ frequency-domain signal vector with $\mathbf{y}_k$ denoting the $N_R \times 1$ received signal vector at the kth subcarriers, and $\mathbf{w}$ is an $N_R N \times 1$ additive white Gaussian noise (AWGN) vector.

3. Phase Noise Effect

It is nontrivial to derive a general expression of PN effects on MIMO-OFDM systems. Instead, we analyze the PN effect for the independent and common oscillator cases (see Figure 3) separately in this section.

3.1. Common Oscillator. When the common oscillator is used at the transmitter and at the receiver, the time-domain input-output relation of the MIMO system at the nth time sample of one OFDM symbol can be expressed as

$$\tilde{\mathbf{y}}(n) = \exp\left(j\beta(n)\right) \sum_{l=0}^{L-1} \mathbf{C}_l \exp\left(j\varphi(n-l)\right) \tilde{\mathbf{x}}(n-l) + \tilde{\mathbf{w}}(n), \tag{3}$$

where $\tilde{\mathbf{x}}(n)$ and $\tilde{\mathbf{y}}(n)$ are $N_T \times 1$ and $N_R \times 1$ vectors consisting of the transmit and receive signals from all the antennas, respectively, $\varphi(n)$ and $\beta(n)$ denote the phase noises of the common oscillators at the transmitter and at the receiver, respectively, $\mathbf{C}_l$ is an $N_R \times N_T$ MIMO channel impulse response (CIR) matrix of the lth tap, and $\tilde{\mathbf{w}}(n)$ is an $N_R \times 1$ vector consisting of the AWGNs.

In the frequency-flat fading channel, (3) reduces to

$$\tilde{\mathbf{y}}(n) = \exp\left(j\beta(n)\right) \exp\left(j\varphi(n)\right) \mathbf{C}_0 \tilde{\mathbf{x}}(n) + \tilde{\mathbf{w}}(n). \tag{4}$$

It is self-evident that the phase noises at the transmitter and at the receiver have equal influence on the MIMO-OFDM system in the frequency-flat fading channel. Note that this holds for both (single-stream) beamforming and SVD-based spatial multiplexing MIMO-OFDM systems.

To study the effects of Tx PN and Rx PN on the MIMO-OFDM system in the frequency-selective channel, we resort to the frequency-domain input-output relation. For better illustration, we start the derivation from a single-antenna OFDM system,

$$\mathbf{y}_1 = \mathbf{F}\,\mathrm{diag}\left(\exp\left(j\boldsymbol{\beta}\right)\right)\mathbf{F}^H\mathbf{H}_1\mathbf{F}\,\mathrm{diag}\left(\exp\left(j\boldsymbol{\varphi}\right)\right)\mathbf{F}^H\mathbf{x}_1 + \mathbf{w}_1, \tag{5}$$

where $\mathbf{H}_1$ is a diagonal matrix consisting of the channel transfer functions at all the N subcarriers of one OFDM symbol, $\boldsymbol{\varphi}$ and $\boldsymbol{\beta}$ denote $N \times 1$ vectors consisting of the time-domain Tx PN and Rx PN of one OFDM symbol, respectively, $\mathbf{F}$ denotes an $N \times N$ unitary discrete Fourier transform (DFT) matrix, whose elements are given by $\exp(-j2\pi kl/N)/\sqrt{N}$ $(k, l = 0, \ldots, N-1)$, and $\mathbf{w}_1$ is an $N \times 1$ AWGN vector. The $N \times 1$ frequency-domain transmit signal $\mathbf{x}_1$ is first transformed into time-domain by $\mathbf{F}^H\mathbf{x}_1$, then the Tx PN corrupted (time-domain) signal is transformed back to the frequency domain by $\mathbf{F}\,\mathrm{diag}(\exp(j\boldsymbol{\varphi}))\mathbf{F}^H\mathbf{x}_1$. Similarly, the received frequency-domain signal $\mathbf{H}_1\mathbf{F}\,\mathrm{diag}(\exp(j\boldsymbol{\varphi}))\mathbf{F}^H\mathbf{x}_1$ is first transformed to the time-domain and corrupted by Rx PN and then transformed back to the frequency domain, resulting in the input-output relation (5). Note that (5) only holds approximately since the PN at the cyclic prefix (CP) and the end of the time-domain OFDM symbol are different. Nevertheless, it is a good approximation [16, 21].

For notational convenience, we denote

$$\mathbf{G}_T = \mathbf{F}\,\mathrm{diag}\left(\exp\left(j\boldsymbol{\varphi}\right)\right)\mathbf{F}^H, \qquad \mathbf{G}_R = \mathbf{F}\,\mathrm{diag}\left(\exp\left(j\boldsymbol{\beta}\right)\right)\mathbf{F}^H, \tag{6}$$

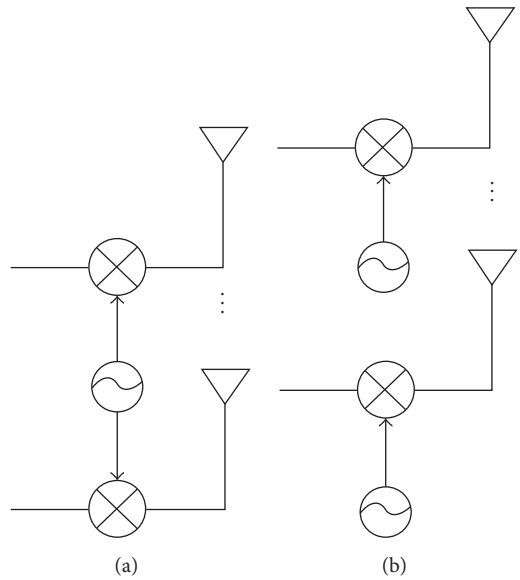

Figure 3: (a) Common oscillator; (b) independent oscillators.

where $\mathbf{G}_{\mathrm{T}}$ takes the form of

$$\mathbf{G}_{\mathrm{T}} = \begin{bmatrix} g_0^{\mathrm{Tx}} & g_{N-1}^{\mathrm{Tx}} & \cdots & g_1^{\mathrm{Tx}} \\ g_1^{\mathrm{Tx}} & g_0^{\mathrm{Tx}} & \cdots & g_2^{\mathrm{Tx}} \\ \vdots & \vdots & \ddots & \vdots \\ g_{N-1}^{\mathrm{Tx}} & g_{N-2}^{\mathrm{Tx}} & \cdots & g_0^{\mathrm{Tx}} \end{bmatrix}. \tag{7}$$

Analogously, the (k,l)th entry of $\mathbf{G}_{\mathrm{R}}$ is $g_{(k-l)_N}^{\mathrm{Rx}}$, where $(k-l)_N$ denotes $(k-l)$ mod N. For an ideal oscillator, $\mathbf{G}_{\mathrm{T}}$ ($\mathbf{G}_{\mathrm{R}}$) boils down to the identity matrix $\mathbf{I}_N$.

The input-output relation for the MIMO-OFDM system can be readily derived as [16]

$$\mathbf{y} = \left(\mathbf{G}_{\mathrm{R}} \otimes \mathbf{I}_{N_{\mathrm{R}}}\right) \mathbf{H} \left(\mathbf{G}_{\mathrm{T}} \otimes \mathbf{I}_{N_{\mathrm{T}}}\right) \mathbf{x} + \mathbf{w}. \tag{8}$$

Let $\mathbf{G}_{\mathrm{T}} = g_0^{\mathrm{Tx}} \mathbf{I}_N + \mathbf{P}_{\mathrm{T}}$ and $\mathbf{G}_{\mathrm{R}} = g_0^{\mathrm{Rx}} \mathbf{I}_N + \mathbf{P}_{\mathrm{R}}$, where $\mathbf{P}_{\mathrm{T}}$ ($\mathbf{P}_{\mathrm{R}}$) contains all the off-diagonal entries of $\mathbf{G}_{\mathrm{T}}$ ($\mathbf{G}_{\mathrm{R}}$) and has zeros at all its diagonal entries, then (8) can be rewritten as

$$\mathbf{y} = g_0^{\mathrm{Rx}} g_0^{\mathrm{Tx}} \mathbf{H}\mathbf{x} + \mathbf{e} + \mathbf{w}, \tag{9}$$

where

$$\begin{aligned} \mathbf{e} = {} & \left(\mathbf{P}_{\mathrm{R}} \otimes \mathbf{I}_{N_{\mathrm{R}}}\right) \mathbf{H} \left(\mathbf{P}_{\mathrm{T}} \otimes \mathbf{I}_{N_{\mathrm{T}}}\right) \mathbf{x} + g_0^{\mathrm{Rx}} \mathbf{H} \left(\mathbf{P}_{\mathrm{T}} \otimes \mathbf{I}_{N_{\mathrm{T}}}\right) \mathbf{x} \\ & + g_0^{\mathrm{Tx}} \left(\mathbf{P}_{\mathrm{R}} \otimes \mathbf{I}_{N_{\mathrm{R}}}\right) \mathbf{H}\mathbf{x}. \end{aligned} \tag{10}$$

Note that, when Tx (Rx) PN is absent, $\mathbf{P}_{\mathrm{T}}$ ($\mathbf{P}_{\mathrm{R}}$) becomes an all zero matrix.

Let the SVD of $\mathbf{H}$ be $\mathbf{H} = \mathbf{U}\mathbf{\Lambda}\mathbf{V}^H$, where $\mathbf{U}, \mathbf{\Lambda}$, and $\mathbf{V}$ are block diagonal matrices, whose kth diagonal block entries are the corresponding SVD of $\mathbf{H}_k$, that is, $\mathbf{U}_k$, $\mathbf{\Lambda}_k$, and $\mathbf{V}_k$. In the sequel, we discuss PN effects on beamforming and spatial multiplexing MIMO-OFDM systems separately.

3.1.1. Beamforming MIMO-OFDM. The transmit and receive beamforming can be expressed as $\mathbf{x} = \widetilde{\mathbf{V}}\mathbf{s}$ and $\mathbf{r} = \widetilde{\mathbf{U}}^H\mathbf{y}$, respectively, where $\mathbf{s}$ and $\mathbf{r}$ are $N \times 1$ vectors of transmit and receive subcarrier signals, and $\widetilde{\mathbf{U}}$ and $\widetilde{\mathbf{V}}$ are block diagonal matrices, whose kth diagonal block entries, $\mathbf{u}_k$ and $\mathbf{v}_k$, are the left and right eigenvectors corresponding to the largest singular value of $\mathbf{H}_k$. Let $\widetilde{\mathbf{\Lambda}}$ be a diagonal matrix consisting of the largest singular values at the N subcarriers. Substituting these parameters into (9) and after simple mathematical arrangement, the estimated signal is obtained as

$$\widehat{\mathbf{s}} = \mathbf{s} + \frac{1}{g_0^{\mathrm{Rx}} g_0^{\mathrm{Tx}}} \widetilde{\mathbf{\Lambda}}^{-1} \widetilde{\mathbf{U}}^H \mathbf{e} + \frac{1}{g_0^{\mathrm{Rx}} g_0^{\mathrm{Tx}}} \widetilde{\mathbf{\Lambda}}^{-1} \widetilde{\mathbf{U}}^H \mathbf{w}. \tag{11}$$

The term $g_0^{\mathrm{Rx}} g_0^{\mathrm{Tx}}$ is the common phase error (CPE) [10] caused by the PN, which can be readily estimated [17]. For the convenience of analysis, we assume the CPE can be estimated perfectly. The 2nd term of the right-hand side (RHS) of (11) corresponds to the intercarrier interference (ICI) [10] caused by the phase noise. The 3rd term of the RHS of (11) is the additive noise. We study ICIs due to Tx PN and Rx PN separately in the sequel.

When there is only Tx PN, (10) boils down to $\mathbf{e} = g_0^{\mathrm{Rx}} \mathbf{H}(\mathbf{P}_{\mathrm{T}} \otimes \mathbf{I}_{N_{\mathrm{T}}})\mathbf{x}$. Substituting it and $\mathbf{x} = \widetilde{\mathbf{V}}\mathbf{s}$ into the 2nd term of the RHS of (11), the ICI caused by the Tx PN can be readily derived as

$$\begin{aligned} \boldsymbol{\xi}_{\mathrm{T}} &= \frac{1}{g_0^{\mathrm{Tx}}} \widetilde{\mathbf{\Lambda}}^{-1} \widetilde{\mathbf{U}}^H \mathbf{H} \left(\mathbf{P}_{\mathrm{T}} \otimes \mathbf{I}_{N_{\mathrm{T}}}\right) \widetilde{\mathbf{V}}\mathbf{s} \\ &= \frac{1}{g_0^{\mathrm{Tx}}} \widetilde{\mathbf{V}}^H \left(\mathbf{P}_{\mathrm{T}} \otimes \mathbf{I}_{N_{\mathrm{T}}}\right) \widetilde{\mathbf{V}}\mathbf{s}. \end{aligned} \tag{12}$$

$\boldsymbol{\xi}_{\mathrm{T}}$ at the kth subcarrier is

$$\xi_{\mathrm{T},k} = \frac{1}{g_0^{\mathrm{Tx}}} \mathbf{v}_k^H \sum_{i=0, i \neq k}^{N-1} g_{(k-i)_N}^{\mathrm{Tx}} \mathbf{v}_i s_i. \tag{13}$$

Assuming independent and identically distributed (i.i.d.) transmit symbol s_i, the power of $\xi_{\mathrm{T},k}$ is

$$J_k^{\mathrm{Tx}} = E\left[\xi_{\mathrm{T},k}^* \xi_{\mathrm{T},k}\right] = \left(\frac{\sigma_s}{g_0^{\mathrm{Tx}}}\right)^2 \sum_{i=0,i\neq k}^{N-1} E\left[\left|g_{(k-i)_N}^{\mathrm{Tx}}\right|^2\right], \quad (14)$$

where E denotes the expectation and $\sigma_s^2 = E[|s_i|^2]$.

Assuming that the ICI and AWGN are independent, the EVM is the ratio of the sum of ICI power and AWGN power to the signal power. The corresponding EVM at the kth subcarrier can be readily derived as

$$\epsilon_k^{\mathrm{Tx}} = \left(\frac{1}{g_0^{\mathrm{Tx}}}\right)^2 \sum_{i=0,i\neq k}^{N-1} E\left[\left|g_{(k-i)_N}^{\mathrm{Tx}}\right|^2\right] + \left(\frac{1}{g_0^{\mathrm{Tx}}}\right)^2 \frac{\sigma_w^2}{\sigma_s^2 \sigma_k^2}, \quad (15)$$

where $\sigma_w^2 = E[|w_i|^2]$ is the variance of the AWGN and σ_k is the largest singular value of $\mathbf{H}_k$.

Similarly, the ICI caused by the Rx PN is given as

$$\begin{aligned}\boldsymbol{\xi}_{\mathrm{R}} &= \frac{1}{g_0^{\mathrm{Rx}}} \widetilde{\boldsymbol{\Lambda}}^{-1} \widetilde{\mathbf{U}}^H \left(\mathbf{P}_{\mathrm{R}} \otimes \mathbf{I}_{N_{\mathrm{R}}}\right) \mathbf{H} \widetilde{\mathbf{V}} \mathbf{s} \\ &= \frac{1}{g_0^{\mathrm{Rx}}} \widetilde{\boldsymbol{\Lambda}}^{-1} \widetilde{\mathbf{U}}^H \left(\mathbf{P}_{\mathrm{R}} \otimes \mathbf{I}_{N_{\mathrm{R}}}\right) \widetilde{\mathbf{U}} \widetilde{\boldsymbol{\Lambda}} \mathbf{s}.\end{aligned} \quad (16)$$

ξ_{R} at the kth subcarrier is

$$\xi_{\mathrm{R},k} = \frac{1}{\sigma_k g_0^{\mathrm{Rx}}} \mathbf{u}_k^H \sum_{i=0,i\neq k}^{N-1} g_{(k-i)_N}^{\mathrm{Rx}} \mathbf{u}_i \sigma_i s_i, \quad (17)$$

whose power is

$$\begin{aligned}J_k^{\mathrm{Rx}} &= E\left[\xi_{\mathrm{R},k}^* \xi_{\mathrm{R},k}\right] \\ &= \left(\frac{\sigma_s}{g_0^{\mathrm{Rx}}}\right)^2 \sum_{i=0,i\neq k}^{N-1} E\left[\left|g_{(k-i)_N}^{\mathrm{Rx}}\right|^2\right] E\left[\frac{\sigma_i^2}{\sigma_k^2}\right],\end{aligned} \quad (18)$$

where σ_i is the largest singular value of $\mathbf{H}_i$. The corresponding EVM is

$$\begin{aligned}\epsilon_k^{\mathrm{Rx}} &= \left(\frac{1}{g_0^{\mathrm{Rx}}}\right)^2 \sum_{i=0,i\neq k}^{N-1} E\left[\left|g_{(k-i)_N}^{\mathrm{Rx}}\right|^2\right] E\left[\frac{\sigma_i^2}{\sigma_k^2}\right] \\ &\quad + \left(\frac{1}{g_0^{\mathrm{Rx}}}\right)^2 \frac{\sigma_w^2}{\sigma_s^2 \sigma_k^2}.\end{aligned} \quad (19)$$

Comparing (14) and (18) or (15) and (19), it is safe to conclude that the ICIs (averaged over all the subcarriers) caused by Tx PN and Rx PN are the same for large N, which holds for practical OFDM systems. Since it suffices to compare the ICI terms of Tx PN and Rx PN, we skip the EVM expressions in the sequel.

3.1.2. Spatial Multiplexing MIMO-OFDM. For the convenience of analysis, we assume the number of spatial stream N_s equals N_{T}, unless otherwise specified. Analogously, the transmit precoder and receive decoder can be expressed as $\mathbf{x} = \mathbf{V}\mathbf{s}$ and $\mathbf{r} = \breve{\mathbf{U}}^H \mathbf{y}$, respectively, where $\mathbf{s}$ and $\mathbf{r}$ are $N_{\mathrm{T}}N \times 1$ vectors of transmit and receive subcarrier signals, and $\breve{\mathbf{U}}$ is a block diagonal matrix, whose kth diagonal block entries $\breve{\mathbf{U}}_k$ are an $N_{\mathrm{R}} \times N_{\mathrm{T}}$ matrix consisting of the left eigenvectors of the N_{T} singular values of $\mathbf{H}_k$. Let $\breve{\boldsymbol{\Lambda}}$ be a diagonal matrix whose kth diagonal block entry consists of the N_{T} singular values of $\mathbf{H}_k$. The estimated signal is

$$\widehat{\mathbf{s}} = \mathbf{s} + \frac{1}{g_0^{\mathrm{Rx}} g_0^{\mathrm{Tx}}} \breve{\boldsymbol{\Lambda}}^{-1} \breve{\mathbf{U}}^H \mathbf{e} + \frac{1}{g_0^{\mathrm{Rx}} g_0^{\mathrm{Tx}}} \breve{\boldsymbol{\Lambda}}^{-1} \breve{\mathbf{U}}^H \mathbf{w}. \quad (20)$$

Substituting $\mathbf{e} = g_0^{\mathrm{Rx}} \mathbf{H}(\mathbf{P}_{\mathrm{T}} \otimes \mathbf{I}_{N_{\mathrm{T}}})\mathbf{x}$ and $\mathbf{x} = \mathbf{V}\mathbf{s}$ into the 2nd term of the RHS of (20), the ICI caused by the Tx PN can be readily derived as

$$\begin{aligned}\boldsymbol{\xi}_{\mathrm{T}} &= \frac{1}{g_0^{\mathrm{Tx}}} \breve{\boldsymbol{\Lambda}}^{-1} \breve{\mathbf{U}}^H \mathbf{H} \left(\mathbf{P}_{\mathrm{T}} \otimes \mathbf{I}_{N_{\mathrm{T}}}\right) \mathbf{V}\mathbf{s} \\ &= \frac{1}{g_0^{\mathrm{Tx}}} \mathbf{V}^H \left(\mathbf{P}_{\mathrm{T}} \otimes \mathbf{I}_{N_{\mathrm{T}}}\right) \mathbf{V}\mathbf{s}.\end{aligned} \quad (21)$$

$\boldsymbol{\xi}_{\mathrm{T}}$ at the kth subcarrier is

$$\boldsymbol{\xi}_{\mathrm{T},k} = \frac{1}{g_0^{\mathrm{Tx}}} \mathbf{V}_k^H \sum_{i=0,i\neq k}^{N-1} g_{(k-i)_N}^{\mathrm{Tx}} \mathbf{V}_i \mathbf{s}_i, \quad (22)$$

where $\mathbf{s}_i$ is an $N_{\mathrm{T}} \times 1$ vector consisting of the transmit signals at the ith subcarrier. The power of $\boldsymbol{\xi}_{\mathrm{T},k}$ is

$$J_k^{\mathrm{Tx}} = E\left[\boldsymbol{\xi}_{\mathrm{T},k}^H \boldsymbol{\xi}_{\mathrm{T},k}\right] = \left(\frac{\sigma_s}{g_0^{\mathrm{Tx}}}\right)^2 N_{\mathrm{T}} \sum_{i=0,i\neq k}^{N-1} E\left[\left|g_{(k-i)_N}^{\mathrm{Tx}}\right|^2\right]. \quad (23)$$

Note that, due to the i.i.d. symbol assumption, $E[\|\mathbf{s}_i\|^2] = \sigma_s^2 N_{\mathrm{T}}$.

Similarly, the ICI caused by the Rx PN is given as

$$\begin{aligned}\boldsymbol{\xi}_{\mathrm{R}} &= \frac{1}{g_0^{\mathrm{Rx}}} \breve{\boldsymbol{\Lambda}}^{-1} \breve{\mathbf{U}}^H \left(\mathbf{P}_{\mathrm{R}} \otimes \mathbf{I}_{N_{\mathrm{R}}}\right) \mathbf{H}\mathbf{V}\mathbf{s} \\ &= \frac{1}{g_0^{\mathrm{Rx}}} \breve{\boldsymbol{\Lambda}}^{-1} \breve{\mathbf{U}}^H \left(\mathbf{P}_{\mathrm{R}} \otimes \mathbf{I}_{N_{\mathrm{R}}}\right) \mathbf{U}\boldsymbol{\Lambda}\mathbf{s}.\end{aligned} \quad (24)$$

$\boldsymbol{\xi}_{\mathrm{R}}$ at the kth subcarrier is

$$\boldsymbol{\xi}_{\mathrm{R},k} = \frac{1}{g_0^{\mathrm{Rx}}} \breve{\boldsymbol{\Lambda}}_k^{-1} \breve{\mathbf{U}}_k^H \sum_{i=0,i\neq k}^{N-1} g_{(k-i)_N}^{\mathrm{Rx}} \mathbf{U}_i \boldsymbol{\Lambda}_i \mathbf{s}_i, \quad (25)$$

whose power is

$$\begin{aligned}J_k^{\mathrm{Rx}} &= \mathrm{tr}\left\{E\left[\boldsymbol{\xi}_{\mathrm{R},k} \boldsymbol{\xi}_{\mathrm{R},k}^H\right]\right\} \\ &= \left(\frac{\sigma_s}{g_0^{\mathrm{Rx}}}\right)^2 N_{\mathrm{T}} \sum_{i=0,i\neq k}^{N-1} E\left[\left|g_{(k-i)_N}^{\mathrm{Rx}}\right|^2\right] \\ &\quad \times \mathrm{tr}\left\{E\left[\mathbf{U}_i \boldsymbol{\Lambda}_i \mathbf{U}_i^H \breve{\mathbf{U}}_k \breve{\boldsymbol{\Lambda}}_k^{-2} \breve{\mathbf{U}}_k^H\right]\right\}.\end{aligned} \quad (26)$$

Assuming i.i.d. subcarrier channels, spatially white MIMO channel [16], and $N_{\mathrm{R}} > N_{\mathrm{T}}$, (26) can be rewritten as

$$\begin{aligned} J_k^{\mathrm{Rx}} &= \left(\frac{\sigma_s}{g_0^{\mathrm{Rx}}}\right)^2 N_{\mathrm{T}} \sum_{i=0, i\neq k}^{N-1} E\left[\left|g_{(k-i)_N}^{\mathrm{Rx}}\right|^2\right] \\ &\quad \times \mathrm{tr}\left\{E\left[\mathbf{U}_i \boldsymbol{\Lambda}_i \mathbf{U}_i^H\right] E\left[\breve{\mathbf{U}}_k \breve{\boldsymbol{\Lambda}}_k^{-2} \breve{\mathbf{U}}_k^H\right]\right\} \\ &= \left(\frac{\sigma_s}{g_0^{\mathrm{Rx}}}\right)^2 \frac{N_{\mathrm{T}}^2}{N_{\mathrm{R}} - N_{\mathrm{T}}} \sum_{i=0, i\neq k}^{N-1} E\left[\left|g_{(k-i)_N}^{\mathrm{Rx}}\right|^2\right]. \end{aligned} \tag{27}$$

The last step in (27) is obtained by recognizing that $E[\mathbf{U}_i \boldsymbol{\Lambda}_i \mathbf{U}_i^H]$ is the correlation matrix at the receiver, which is an identity matrix in spatially white MIMO channels, and that $\breve{\mathbf{U}}_k \breve{\boldsymbol{\Lambda}}_k^{-2} \breve{\mathbf{U}}_k^H$ is an inverse Wishart matrix, whose trace expectation is $N_{\mathrm{T}}/(N_{\mathrm{R}} - N_{\mathrm{T}})$ when $N_{\mathrm{R}} > N_{\mathrm{T}}$ [32].

Comparing (23) and (27), it is found that Tx PN and Rx PN have different influences on SVD-based spatial multiplexing MIMO-OFDM systems. Specifically, (1) the Tx PN has more influence than the Rx PN does when $N_{\mathrm{R}} > 2N_{\mathrm{T}}$; (2) the Rx PN has more influence than the Tx PN does when $N_{\mathrm{T}} < N_{\mathrm{R}} < 2N_{\mathrm{T}}$; (3) Tx PN and Rx PN have the same influence when $N_{\mathrm{R}} = 2N_{\mathrm{T}}$. Interestingly, the same conclusions were drawn in [16] for open-loop MIMO-OFDM systems with spatial multiplexing and ZF decoder. Note that, when $N_{\mathrm{R}} = N_{\mathrm{T}}$, the expectation of the inverse Wishart matrix does not exist [32]. Thus, there is no analytical expression for the ICI power due to Rx PN when $N_{\mathrm{R}} = N_{\mathrm{T}}$. (Due to the singularity in (27), simulations for the $N_{\mathrm{R}} = N_{\mathrm{T}}$ case do not converge.)

It should be noted that (27) is only valid under the assumptions of i.i.d. subcarrier channels and spatially white MIMO channels. In practice, the channels may be correlated in both frequency and spatial domains. Nevertheless, the spatial correlation can be reduced with sufficient antenna spacing and scattering; the time correlation diminishes when the channel length is comparable to the OFDM symbol and the channel taps are uncorrelated. Moreover, these assumptions allow more insight into the PN impairments and the findings hold for arbitrary MIMO channels in general. To demonstrate this, a spatially correlated MIMO channel is studied by simulations in Section 4.

3.2. Independent Oscillator. For simplicity, we consider the frequency-flat fading channel for the independent oscillator case. Although the independent oscillator results are derived from the frequency-flat fading channel, as will be shown by simulations in the next section, it holds for frequency-selective fading as well.

When each antenna is equipped with an independent oscillator, the received time-domain signal can be expressed as

$$\begin{aligned} &\widetilde{\mathbf{y}}(n) \\ &\quad = \mathrm{diag}\left(\exp\left(j\widetilde{\boldsymbol{\beta}}(n)\right)\right) \mathbf{C}_0 \,\mathrm{diag}\left(\exp\left(j\widetilde{\boldsymbol{\varphi}}(n)\right)\right) \widetilde{\mathbf{x}}(n) \\ &\qquad + \widetilde{\mathbf{w}}(n), \end{aligned} \tag{28}$$

where $\widetilde{\boldsymbol{\varphi}}(n)$ and $\widetilde{\boldsymbol{\beta}}(n)$ are $N_{\mathrm{T}} \times 1$ and $N_{\mathrm{R}} \times 1$ vectors consisting of the nth samples of phase noises at the transmit and receive antennas, respectively. For notational convenience, we drop the time index n hereafter.

3.2.1. Beamforming MIMO. After transmit and receive beamforming, the estimated signal can be readily derived from (28) as

$$\begin{aligned} \widehat{s} &= \sigma^{-1} \mathbf{u}^H \mathrm{diag}\left(\exp\left(j\widetilde{\boldsymbol{\beta}}\right)\right) \mathbf{C}_0 \,\mathrm{diag}\left(\exp\left(j\widetilde{\boldsymbol{\varphi}}\right)\right) \mathbf{v} s \\ &\quad + \sigma^{-1} \mathbf{u}^H \widetilde{\mathbf{w}}, \end{aligned} \tag{29}$$

where $\mathbf{u}$ and $\mathbf{v}$ are the eigenvectors corresponding to the largest singular value of $\mathbf{C}_0, \sigma$. The first term of the RHS of (29) can be rewritten as

$$\left(\sum_{m=1}^{N_{\mathrm{R}}} \exp\left(j\beta_m\right) |u_m|^2\right) \left(\sum_{n=1}^{N_{\mathrm{T}}} \exp\left(j\varphi_n\right) |v_n|^2\right) s. \tag{30}$$

Although the PN at mmWave frequencies is more severe, thanks to the PLL, the PN value (i.e., each realization of the random variable PN) is still much smaller than 1 [9]. Hence, the first-order Taylor expansion can be used; that is, $\exp(j\varphi_n) \approx 1 + j\varphi_n$ and $\exp(j\beta_m) \approx 1 + j\beta_m$. (The Taylor expansion for small PN has been widely used in the literature. Nevertheless, it should be noted that the Taylor expansion may not be applicable to the PN of a free-running oscillator, whose variance increases linearly with time, after long transmission.) As a result, (30) can be approximated as

$$\begin{aligned} &s + \left(j \sum_{m=1}^{N_{\mathrm{R}}} \beta_m |u_m|^2 + j \sum_{n=1}^{N_{\mathrm{T}}} \varphi_n |v_n|^2 \right. \\ &\qquad \left. - \sum_{m=1}^{N_{\mathrm{R}}} \beta_m |u_m|^2 \sum_{n=1}^{N_{\mathrm{T}}} \varphi_n |v_n|^2\right) s, \end{aligned} \tag{31}$$

where the second term represents the PN impairment. It can be seen from (31) that, for the independent oscillator case, the PN effect on beamforming MIMO systems can be reduced by having more antennas at either side since the phase noises at different antennas are independent. The Rx PN has more influence than the Tx PN when $N_{\mathrm{T}} > N_{\mathrm{R}}$, the Tx PN and the Rx PN have the same influence when $N_{\mathrm{R}} = N_{\mathrm{T}}$, and the Tx PN has more influence than the Rx PN side when $N_{\mathrm{R}} > N_{\mathrm{T}}$.

3.2.2. Spatial Multiplexing MIMO. After SVD precoding and decoding, the estimated signals can be readily derived from (28) as

$$\begin{aligned} &\widehat{\mathbf{s}} \\ &\quad = \boldsymbol{\Lambda}_c^{-1} \mathbf{U}_c^H \mathbf{u}^H \mathrm{diag}\left(\exp\left(j\widetilde{\boldsymbol{\beta}}\right)\right) \mathbf{C}_0 \,\mathrm{diag}\left(\exp\left(j\widetilde{\boldsymbol{\varphi}}\right)\right) \mathbf{V}_c \mathbf{s} \\ &\qquad + \boldsymbol{\Lambda}_c^{-1} \mathbf{U}_c^H \widetilde{\mathbf{w}}, \end{aligned} \tag{32}$$

where $\mathbf{U}_c$, $\mathbf{\Lambda}_c$, and $\mathbf{V}_c$, are SVD of $\mathbf{C}_0$. The first term of the RHS of (32) can be rewritten as $\mathbf{\Xi s}$, where $\mathbf{\Xi}$ is a diagonal matrix whose ith diagonal element is

$$\left(\sum_{m=1}^{N_R} \exp\left(j\beta_m\right)\left|u_{im}\right|^2\right)\left(\sum_{n=1}^{N_T} \exp\left(j\varphi_n\right)\left|v_{in}\right|^2\right)s_i, \quad (33)$$

with u_{im} and v_{in} denoting the (i,m)th and (i,n)th elements of $\mathbf{U}$ and $\mathbf{V}$, respectively. Following the same lines as in the previous subsection, that is, $\exp(j\varphi_n) \approx 1 + j\varphi_n$ and $\exp(j\beta_m) \approx 1 + j\beta_m$, (33) can be approximated as

$$s_i + \left(j\sum_{m=1}^{N_R}\beta_m\left|u_{im}\right|^2 + j\sum_{n=1}^{N_T}\varphi_n\left|v_{in}\right|^2 - \sum_{m=1}^{N_R}\beta_m\left|u_{im}\right|^2\sum_{n=1}^{N_T}\varphi_n\left|v_{in}\right|^2\right)s_i. \quad (34)$$

As can be seen, the PN effect of independent oscillators on spatial multiplexing MIMO systems can be reduced by having more antennas.

Even though spatially white MIMO channels are assumed in this section for tractable analysis, the analysis also holds for spatially correlated MIMO channels. Moreover, by regarding each antenna in the analysis as a (analog) phase-controlled subarray in hybrid beamforming, the findings are also applicable to hybrid beamforming. These observations will be demonstrated by simulations in the next section.

4. Simulation

Throughout the simulations, we assume $N = 1024$ subcarriers, including $N_a = 834$ active subcarriers, $N_g = 158$ guard band subcarriers (79 zero subcarriers in the beginning and end of each OFDM symbol), $N_p = 32$ number of scattered pilots, 16 quadrature amplitude modulation (16-QAM), 240-MHz useful bandwidth (sampling frequency of about 284 MHz), and 60-GHz carrier frequency. The phase noise model of the PLL-based oscillator (cf. Section 2.1) (in the "high" mode [7]) is employed. The CP length is set to be no smaller than the channel length. The CSI is assumed to be known at the transmitter and at the receiver. For simplicity, we assume spatially white MIMO channels throughout this section, unless otherwise specified.

4.1. Common Oscillator. The EVM performances of an 8×4 ($N_R \times N_T$) beamforming MIMO-OFDM system with a common oscillator at the transmitter (Tx PN) and at the receiver (Rx PN) in frequency-flat and frequency-selective Rayleigh fading channels are shown in Figure 4. As a reference, the ideal oscillator case (no PN) is also shown in the plot. As can be seen, the Tx PN and the Rx PN of the common oscillator have the same influence on the beamforming MIMO-OFDM system. Note that the mmWave channel is sparse, thus it can be modeled by a few taps [33]. In this work, a 4-tap Rayleigh fading channel (whose taps are at the 0, 20, 30, and 60th time samples with equal average tap gain) is chosen as the frequency-selective channel. (Without further specification, frequency-selective channels in this section refer to this model.) As the analysis in the previous section is general for any frequency-selective channel, the conclusions drawn here hold for frequency-selective fading channels with any number of taps. For the sake of conciseness, results of frequency-selective channels with different numbers of taps are not shown in this paper.

For simplicity, we have assumed spatially white MIMO channels. Nevertheless, the conclusion also holds for spatially correlated MIMO channels. To demonstrate this, we assume a uniform linear array with half-wavelength interelement distance at both Tx and Rx and introduce antenna correlations at both sides using the Kronecker channel model with the Bessel correlation function $J_0(2\pi d_{mn}/\lambda)$ [34], where J_0 is the zeroth-order Bessel function of the first kind, d_{mn} is the distance between the mth and nth antenna elements in the Tx (or Rx) array, and λ is the wavelength. The corresponding results are shown in Figure 4(c). As can be seen, with spatial correlations, the EVM performance degrades, however, the Tx PN and the Rx PN of the common oscillator still have the same influence on the beamforming OFDM system. For the sake of conciseness, results of spatially correlated MIMO channels are not shown in the sequel, except for simulations of hybrid beamforming with a sophisticated mmWave channel model in Section 4.2.

In order to verify the effects of Tx PN and Rx PN on SVD-based spatial multiplexing MIMO-OFDM systems (Section 3.1.2), we generate i.i.d. subcarrier channels (with a channel length of N) and set the CP length to N. Figure 5 shows EVM performances of 3×2, 4×2, and 5×2 MIMO systems. As can be seen, the Rx PN has more influence than the Tx PN does when $N_T = 2 < N_R = 3 < 2N_T = 4$; Tx PN and Rx PN have the same influence when $N_R = 4 = 2N_T$; the Tx PN has more influence than the Rx PN does when $N_R = 5 > 2N_T = 4$.

4.2. Independent Oscillator. Figure 6 shows the EVM performances of 8×4 and 4×8 beamforming MIMO-OFDM with independent oscillators in the frequency-selective Rayleigh fading channel. As can be seen, the Tx PN has more influence (than the Rx PN) on the 8×4 beamforming MIMO-OFDM system and less influence (than the Rx PN) on the 4×8 beamforming MIMO-OFDM system. This is because PNs of independent oscillators (at either side) are reduced by averaging over the antennas (cf. Section 3.2). In Figure 6(a), the Tx PN has more influence because there are more receive antennas than transmit antennas. Similarly, in Figure 6(b), the Rx PN has more influence because there are more transmit antennas than receive antennas.

As mentioned before, by regarding each antenna in the analysis as a (analog) phase-controlled subarray in hybrid beamforming, the findings are also applicable to hybrid beamforming. To verify this, we run simulations of a hybrid beamforming system with independent oscillators using the QuaDRiGa channel model [35]. The QuaDRiGa model is a three-dimensional geometry-based stochastic channel model that is under constant development. Its current version allows

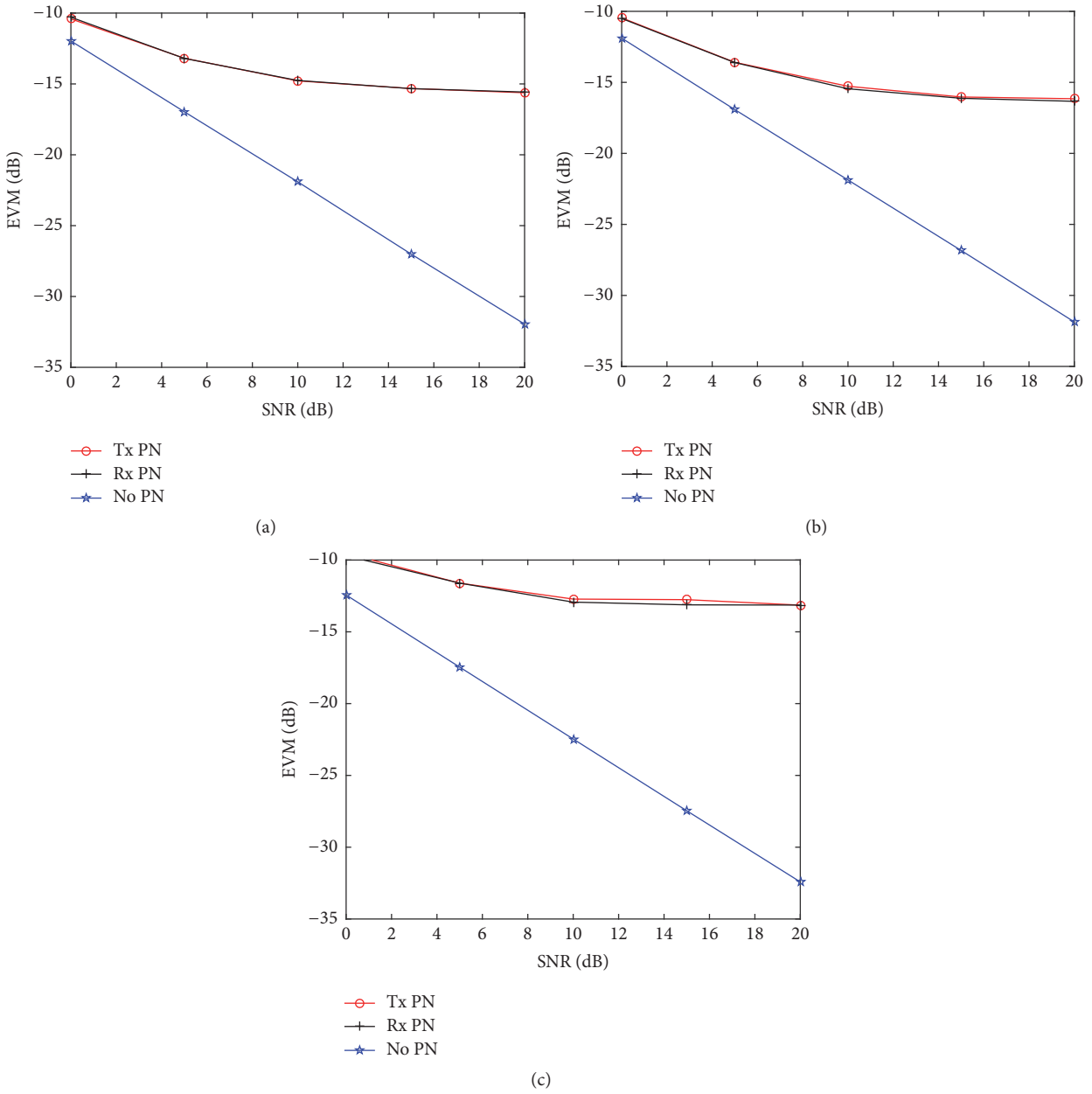

Figure 4: EVM performances of an 8 × 4 beamforming MIMO-OFDM with common oscillators in (a) frequency-flat fading channel, (b) frequency-selective fading channel, and (c) spatially correlated frequency-selective fading channel.

channel simulations up to 100-GHz carrier frequency. Accurate as it is, the channel emulation can be time-consuming, especially for large antenna arrays. In order to focus on the PN effects and to reduce simulation time, we assume 8 and 16 antenna elements as Tx and Rx arrays (both with perfect channel state information), and vice versa. (In practice, the channels can be estimated using adaptive compressive sensing algorithms [5].) We further assume one radio frequency (RF) chain is connected to a subarray of 4 antenna elements and each subarray is a uniform linear array with half-wavelength interelement distance. That is, there are 2 and 4 RF chains at Tx and Rx, and vice versa. Figure 7 shows the simulated results. The same conclusions are drawn; that is, the effects of PNs of independent oscillators at Tx (Rx) side are alleviated with more Tx (Rx) antennas.

In order to demonstrate the antenna averaging effect on the phase noises of independent oscillators, we simulate an $N_R \times 1$ receive beamforming OFDM system with different numbers of receive antennas and a $4 \times N_T$ SVD-based spatial multiplexing OFDM system with different numbers of transmit antennas at 15-dB signal-to-noise ratio (SNR) in frequency-selective fading channels. Figure 8(a) shows that the influence of the Rx PN reduces by increasing N_R, whereas the influence of Tx PN stays almost the same with increasing N_R. Similar conclusions can be drawn for the Tx PN effect on the $4 \times N_T$ spatial multiplexing OFDM system (where the

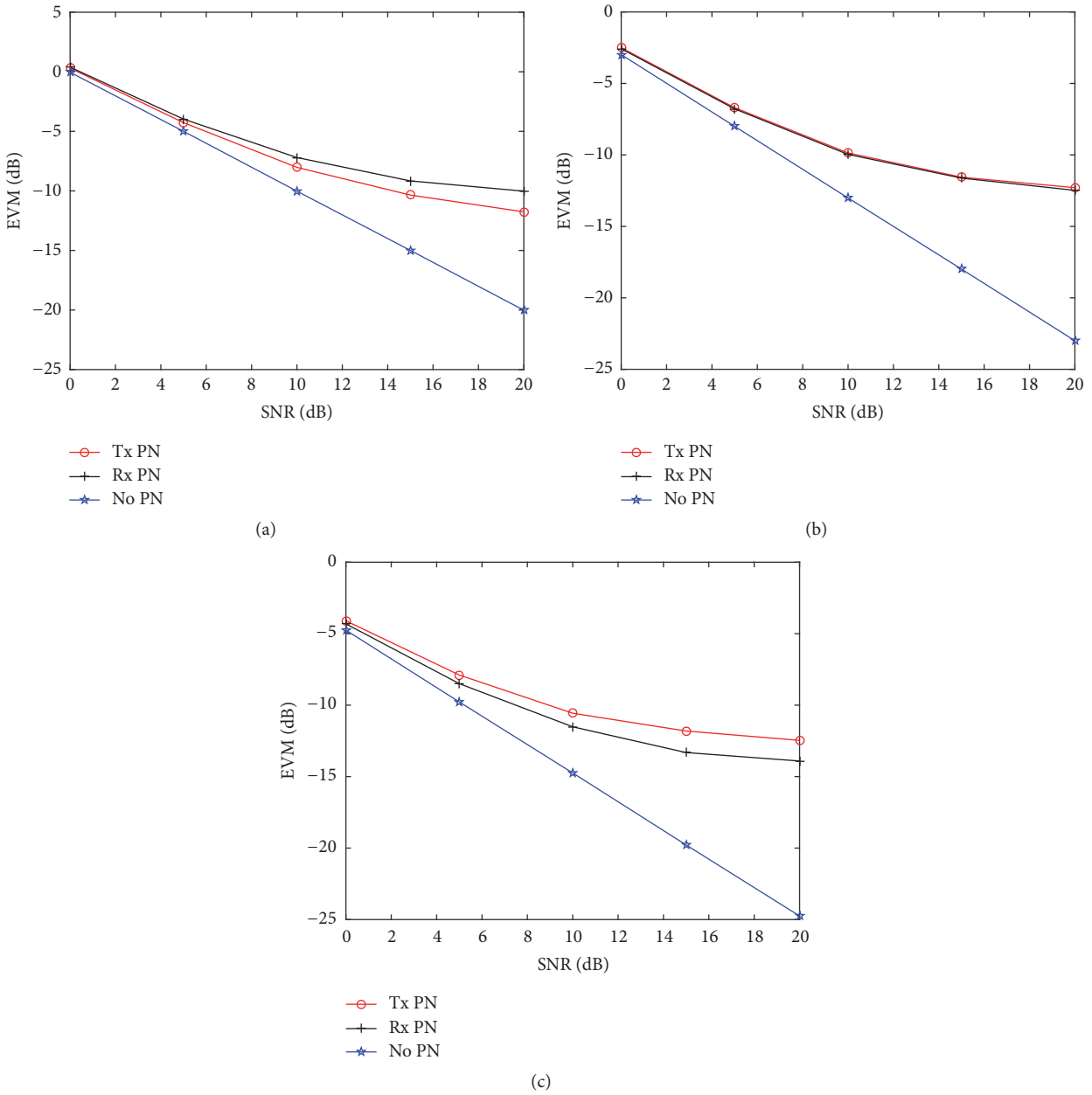

FIGURE 5: EVM performances of SVD-based spatial multiplexing MIMO-OFDM system with common oscillators in i.i.d. subcarrier channels: (a) 3×2 MIMO system; (b) 4×2 MIMO system; (c) 5×2 MIMO system.

number of spatial streams is set to 4); see Figure 8(b); that is, the influence of the Tx PN reduces by increasing N_T, whereas the influence of Rx PN stays almost the same with increasing N_T.

Figure 9 shows the EVM performances of beamforming OFDM systems without any phase noise correction (no correction) and with CPE correction, for the common oscillator and independent oscillator cases. (For the common oscillator case, the scalar CPE can be estimated and corrected using the standard CPE correlation algorithm [17], whereas, for the independent oscillator case, the CPEs of the independent oscillators can be jointly corrected using the CPE correction algorithm.) It can be seen that the independent oscillator case has better EVM performance than the common oscillator case. Note that, for the conciseness of the paper, we only present the results for beamforming OFDM systems in this paper, while the same conclusion can be drawn for the spatial multiplexing case.

5. Conclusion

In this paper, the phase noise (PN) effects on beamforming MIMO-OFDM systems were investigated. We showed that, in frequency-selective fading channels, the PNs of common

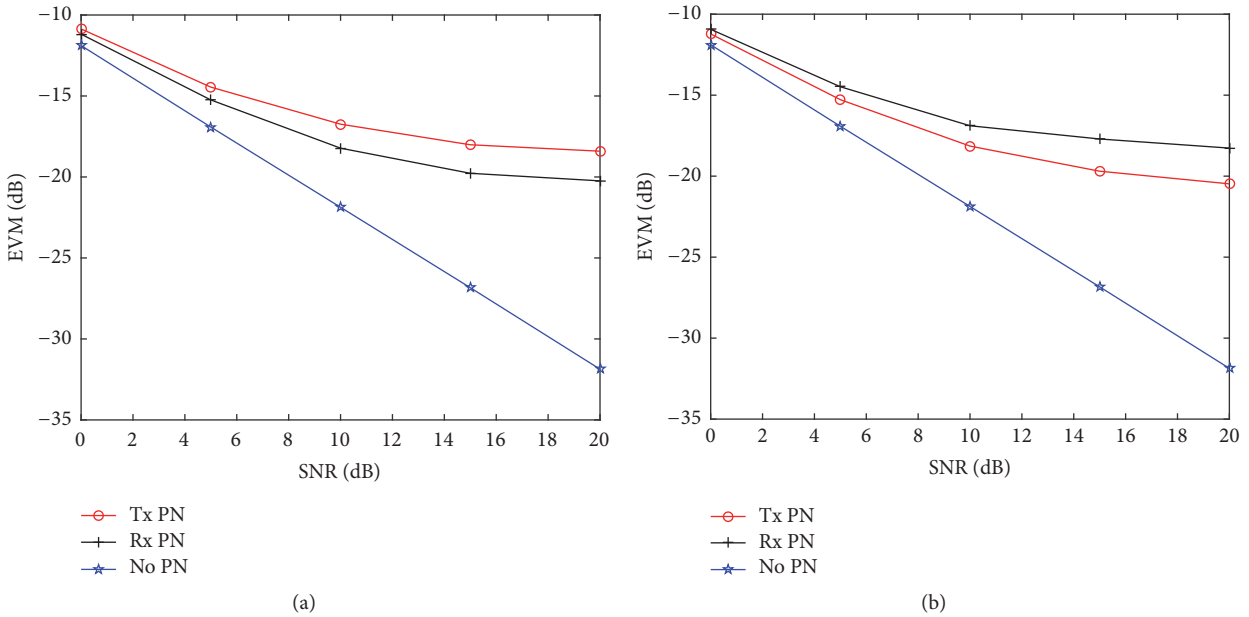

Figure 6: EVM performances of (a) 8 × 4 and (b) 4 × 8 beamforming MIMO-OFDM with independent oscillators in frequency-selective fading channel.

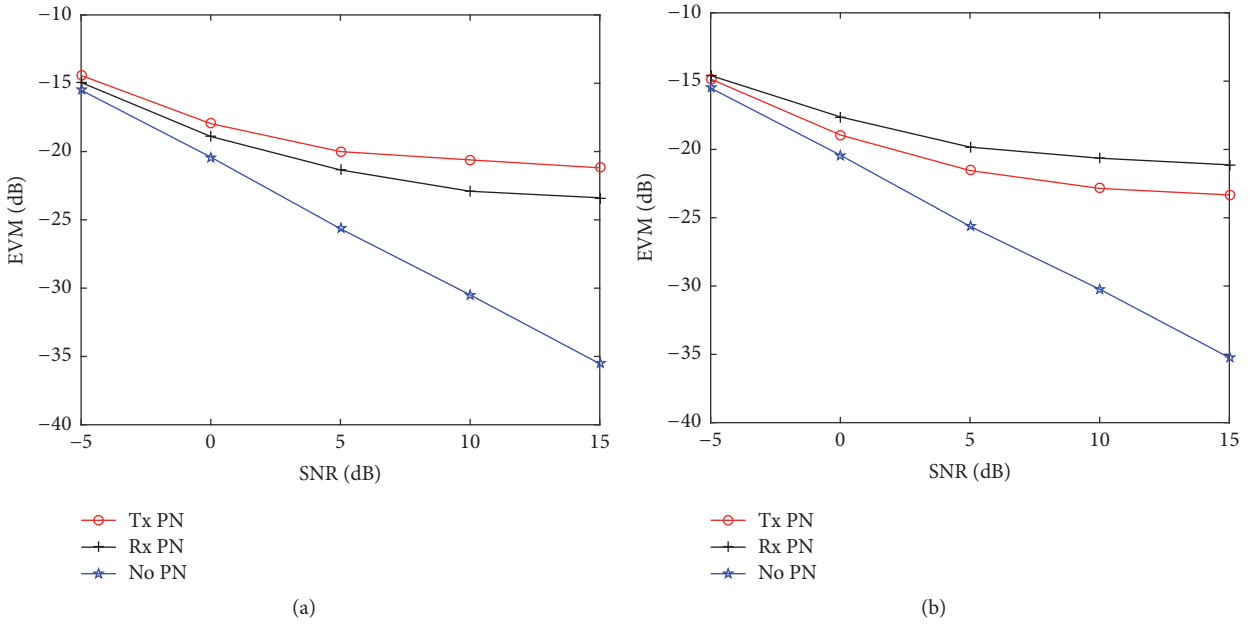

Figure 7: EVM performances of (a) 16 × 8 and (b) 8 × 16 hybrid beamforming MIMO-OFDM with independent oscillators in mmWave channel.

oscillators at the transmitter and at the receiver have the same influence on (single-stream) beamforming OFDM systems, yet different influences on spatial multiplexing OFDM systems. For the independent oscillator case, however, it was shown that the phase noise effect at either side can be alleviated by having more antennas for both beamforming and spatial multiplexing OFDM systems. It was also shown that the independent oscillator case can have better error vector magnitude (EVM) performance than the common oscillator case for MIMO-OFDM systems. Simulations show that the analysis holds not only for spatially white/correlated MIMO channels, but also for hybrid beamforming in mmWave channels.

Conflicts of Interest

The authors declare that they have no conflicts of interest.

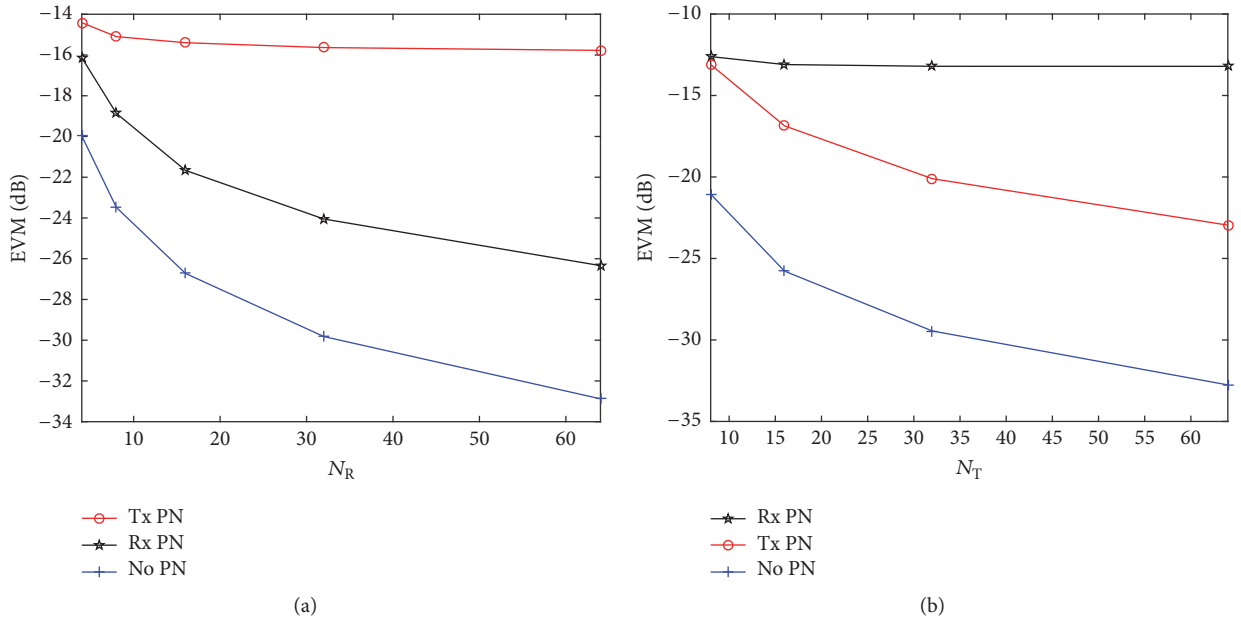

FIGURE 8: EVM performances of MIMO-OFDM system with independent oscillators at 15-dB SNR in frequency-selective fading channel: (a) $N_R \times 1$ receive beamforming; (b) $4 \times N_T$ SVD-based spatial multiplexing.

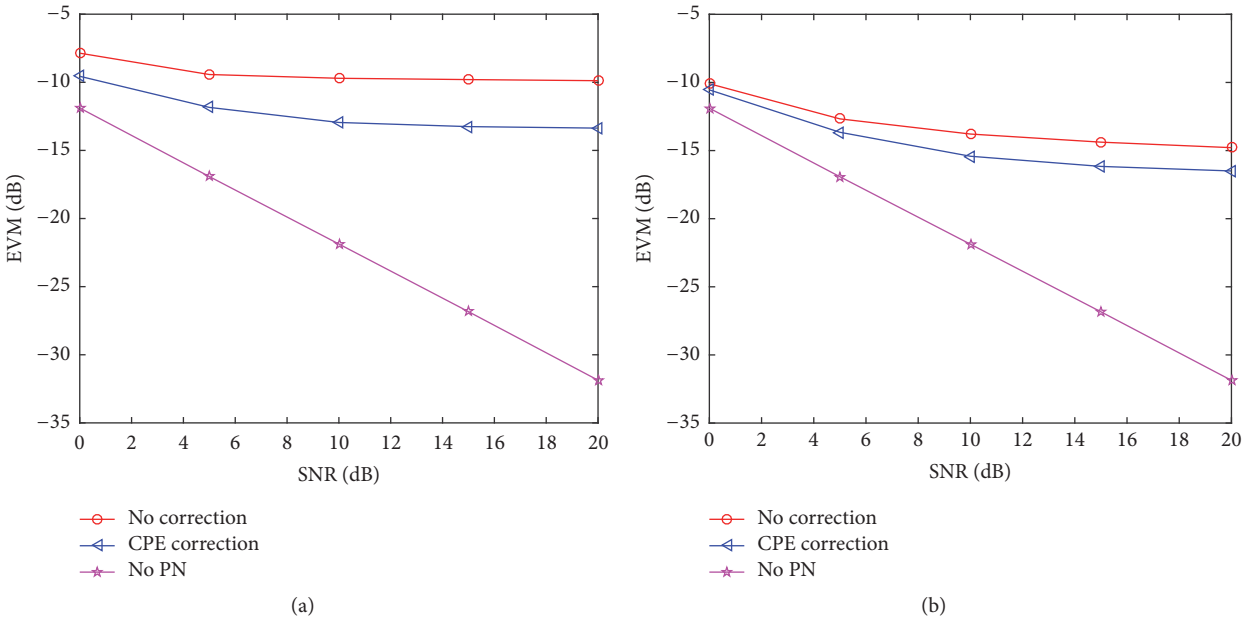

FIGURE 9: EVM performances of 8×4 beamforming MIMO-OFDM with both Tx PN and Rx PN in frequency-selective fading channel: (a) the common oscillator case; (b) the independent oscillator case.

Acknowledgments

The research leading to these results received funding from the European Commission H2020 Programme under Grant Agreement no. 671650 (5G PPP mmMAGIC project).

References

[1] P. F. M. Smulders, "Statistical characterization of 60-GHz indoor radio channels," *IEEE Transactions on Antennas and Propagation*, vol. 57, no. 10, pp. 2820–2829, 2009.

[2] R. He, Z. Zhong, B. Ai, and J. Ding, "An empirical path loss model and fading analysis for high-speed railway viaduct scenarios," *IEEE Antennas and Wireless Propagation Letters*, vol. 10, pp. 808–812, 2011.

[3] K. Guan, B. Ai, A. Fricke et al., "Excess Propagation Loss of Semi-Closed Obstacles for Inter/Intra-Device Communications in the Millimeter-Wave Range," *Journal of Infrared, Millimeter, and Terahertz Waves*, vol. 37, no. 7, pp. 676–690, 2016.

[4] K. Guan, G. Li, T. Kuerner et al., "On millimeter wave and THz mobile radio channel for smart rail mobility," *IEEE Transactions on Vehicular Technology*, vol. 66, no. 7, pp. 5658–5674, 2016.

[5] A. Alkhateeb, J. Mo, N. González-Prelcic, and R. W. Heath Jr., "MIMO precoding and combining solutions for millimeter-wave systems," *IEEE Communications Magazine*, vol. 52, no. 12, pp. 122–131, 2014.

[6] A. A. Zaidi, J. Luo, R. Gerzaguet et al., "Evaluation of waveforms for mobile radio communications above 6 GHz," in *Proceedings of the 2016 IEEE Globecom Workshops*, Washington, DC, USA, December 2016.

[7] http://www.3gpp.org/.

[8] A. Demir, "Computing timing jitter from phase noise spectra for oscillators and phase-locked loops with white and 1/f noise," *IEEE Transactions on Circuits and Systems I: Regular Papers*, vol. 53, no. 9, pp. 1869–1884, 2006.

[9] P. Zetterberg, A. Wolfgang, A. Westlund et al., Initial multi-node and antenna transmitter and receiver architectures and schemes," mmMAGIC Deliverable D5.1, June 2016, https://bscw.5g-mmmagic.eu/pub/bscw.cgi/d95056/mmMAGIC_D5_1.pdf.

[10] D. Petrovic, W. Rave, and G. Fettweis, "Effects of phase noise on OFDM systems with and without PLL: Characterization and compensation," *IEEE Transactions on Communications*, vol. 55, no. 8, pp. 1607–1616, 2007.

[11] Q. Zou, A. Tarighat, and A. H. Sayed, "Compensation of phase noise in OFDM wireless systems," *IEEE Transactions on Signal Processing*, vol. 55, no. 11, pp. 5407–5424, 2007.

[12] A. Puglielli, G. Lacaille, A. M. Niknejad, G. Wright, B. Nikolic, and E. Alon, "Phase noise scaling and tracking in OFDM multi-user beamforming arrays," in *Proceedings of the 2016 IEEE International Conference on Communications (ICC '16)*, 6, 1 pages, Kuala Lumpur, Malaysia, May 2016.

[13] P. Mathecken, T. Riihonen, N. N. Tchamov, S. Werner, M. Valkama, and R. Wichman, "Characterization of OFDM radio link under PLL-based oscillator phase noise and multipath fading channel," *IEEE Transactions on Communications*, vol. 60, no. 6, pp. 1479–1485, 2012.

[14] A. Gokceoglu, Y. Zou, M. Valkama, P. C. Sofotasios, P. Mathecken, and D. Cabric, "Mutual information analysis of OFDM radio link under phase noise, IQ imbalance and frequency-selective fading channel," *IEEE Transactions on Wireless Communications*, vol. 12, no. 6, pp. 3048–3059, 2013.

[15] X. Chen, A. Wolfgang, and A. Zaidi, "MIMO-OFDM for small cell backhaul in the presence of synchronization errors and phase noise," in *Proceedings of the 2017 IEEE International Conference on Communications Workshops (ICC Workshops)*, pp. 1221–1226, Paris, France, May 2017.

[16] T. C. W. Schenk, X.-J. Tao, P. F. M. Smulders, and E. R. Fledderus, "On the influence of phase noise induced ICI in MIMO OFDM systems," *IEEE Communications Letters*, vol. 9, no. 8, pp. 682–684, 2005.

[17] P. Liu, S. Wu, and Y. Bar-Ness, "A phase noise mitigation scheme for MIMO WLANs with spatially correlated and imperfectly estimated channels," *IEEE Communications Letters*, vol. 10, no. 3, pp. 141–143, 2006.

[18] S. Bittner, E. Zimmermann, and G. Fettweis, "Exploiting phase noise properties in the design of MIMO-OFDM receivers," in *Proceedings of the IEEE Wireless Communications and Networking Conference (WCNC '08)*, pp. 940–945, Las Vegas, NV, USA, March 2008.

[19] R. Corvaja and A. G. Armada, "SINR degradation in MIMO-OFDM systems with channel estimation errors and partial phase noise compensation," *IEEE Transactions on Communications*, vol. 58, no. 8, pp. 2199–2203, 2010.

[20] Y. Zhang and H. Liu, "MIMO-OFDM systems in the presence of phase noise and doubly selective fading," *IEEE Transactions on Vehicular Technology*, vol. 56, no. 4, pp. 2277–2285, 2007.

[21] R. Hamila, Ö. Özdemir, and N. Al-Dhahir, "Beamforming OFDM Performance Under Joint Phase Noise and I/Q Imbalance," *IEEE Transactions on Vehicular Technology*, vol. 65, no. 5, pp. 2978–2989, 2016.

[22] S. Stefanatos, F. Foukalas, and T. Khattab, "On the Achievable Rates of OFDM with Common Phase Error Compensation in Phase Noise Channels," *IEEE Transactions on Communications*, vol. 65, no. 8, pp. 3509–3521, 2017.

[23] T.-J. Lee and Y.-C. Ko, "Channel estimation and data detection in the presence of phase noise in MIMO-OFDM systems with independent oscillators," *IEEE Access*, vol. 5, pp. 9647–9662, 2017.

[24] P. Xu, Y. Xiao, S. Zhou, and M. Zhao, "ICI analysis of MIMO-OFDM systems with independent phase noise at both transmit and receive antennas," in *Proceedings of the 5th International Conference on Wireless Communications, Networking and Mobile Computing (WiCOM '09)*, Beijing, China, September 2009.

[25] R. Krishnan, M. R. Khanzadi, and N. Krishnan, On the impact of oscillator phase noise on the uplink performance in a massive MIMO-OFDM system, arxiv.org/abs/1405.0669, 2014.

[26] T. Höhne and V. Ranki, "Phase noise in beamforming," *IEEE Transactions on Wireless Communications*, vol. 9, no. 12, pp. 3682–3689, 2015.

[27] A. Pitarokoilis, S. K. Mohammed, and E. G. Larsson, "Uplink performance of time-reversal MRC in Massive MIMO systems subject to phase noise," *IEEE Transactions on Wireless Communications*, vol. 14, no. 2, pp. 711–723, 2015.

[28] A. Georgiadis, "Gain, phase imbalance, and phase noise effects on error vector magnitude," *IEEE Transactions on Vehicular Technology*, vol. 53, no. 2, pp. 443–449, 2004.

[29] X. Chen, C. Fang, Y. Zou, A. Wolfgang, and T. Svensson, "Beamforming MIMO-OFDM Systems in the Presence of Phase Noises at Millimeter-Wave Frequencies," in *Proceedings of the 2017 IEEE Wireless Communications and Networking Conference Workshops (WCNCW)*, pp. 1–6, San Francisco, CA, USA, March 2017.

[30] S. Chen, S. Sun, Q. Gao, and X. Su, "Adaptive beamforming in TDD-based mobile communication systems: State of the art and 5G research directions," *IEEE Wireless Communications Magazine*, vol. 23, no. 6, pp. 81–87, 2016.

[31] P. Graczyk, G. Letac, and H. Massam, "The complex Wishart distribution and the symmetric group," *The Annals of Statistics*, vol. 31, no. 1, pp. 287–309, 2003.

[32] W. Fan, I. Carton, J. Ø. Nielsen, K. Olesen, and G. F. Pedersen, "Measured wideband characteristics of indoor channels at centimetric and millimetric bands," *EURASIP Journal on Wireless Communications and Networking*, vol. 2016, no. 1, article no. 58, pp. 1–13, 2016.

[33] A. Paulraj, R. Nabar, and D. Gore, *Introduction to Space-time Wireless Communication*, Cambridge University Press, 2003.

[34] S. Jaeckel, L. Raschkowski, K. Borner, and L. Thiele, "QuaDRiGa: a 3-D multi-cell channel model with time evolution for enabling virtual field trials," *IEEE Transactions on Antennas and Propagation*, vol. 62, no. 6, pp. 3242–3256, 2014.

[35] S. Wu and Y. Bar-Ness, "Multiple phase noise correction for OFDM/SDMA," in *Proceedings of the GLOBECOM '03. IEEE Global Telecommunications Conference*, pp. 1311–1315, San Francisco, CA, USA.